

DETC2006-99671

STRUCTURAL DYNAMICS AND SYSTEM IDENTIFICATION OF PARALLEL KINEMATIC MACHINES

Gloria J. Wiens

Dept. of Mechanical and Aerospace Engineering
University of Florida
Gainesville, FL 32611-6250
gwiens@ufl.edu

David S. Hardage

Dept. of Mechanical and Aerospace Engineering
University of Florida
Gainesville, FL 32611-6250

ABSTRACT

One of the primary concerns associated with the machining process involves excess vibrations that can adversely affect the ability of the machine tool to accurately produce parts. This paper presents the development of a method by which the vibrational characteristics of machine tools exhibiting a parallel kinematic machine architecture may be modeled. Theoretical and experimental results are compared to demonstrate the validity of the modeling approach. The resulting model provides an effective means to guide the machine design process for the purposes of enhancing performance and improving control.

INTRODUCTION

Throughout recent years, the evolution of machine tools has been facilitated by technological advances in manufacturing methods and changing design philosophies, and has led to a number of innovative parallel machine architectures that deviate from those of the conventional serial mechanism [1]. Manufacturers of these machine tools and proponents of PKMs for use in machining applications have long maintained that one of the intrinsic characteristics of the parallel manipulator is a comparatively high stiffness. However, recent speculation has suggested that for any conceivable mechanism pose, there is at least one direction in which the stiffness at the platform is less than the stiffness of one of the links [2]. Furthermore, vibrations induced through the excitation of structural modes can produce deviations in the nominal tool path while machining which will result in errors in the workpiece surface. A model for predicting the structural dynamic response of a PKM would provide the means for identifying regions and directions of low stiffness in the workspace that could potentially result in excessive vibration of

the structure. Knowledge of these regions and/or directions would also give insight into the contributions of the various mechanical components to the vibrational response.

As evidence by the literature, or lack of it, the dynamic modeling of parallel kinematic machines (PKM) is slowly being addressed. For the PKM, their rigid body equations of motion have evolved from initial models that employed simplifying assumptions such as considering the link masses to be point masses located at the geometric center of the links [3], to more complicated forms that consider the effects of link inertia [4, 5] and viscous and Coulomb friction in the joints [5, 6]. Other researchers have evoked in their modeling special kinematic configurations such as the 6-6 Serial Parallel Mechanism (SPM) [7] and a 3 degree of freedom parallel manipulator resembling a SPM [8]. Due to the presence of closed-loop kinematic chains inherent to PKMs, the Kane's method has been used in several works [5, 9-11].

Although the preceding derivations are based on the assumption of rigid bodies, contributions due to the flexibility of the links [12] have also been taken into account. In one case [13], the dynamic equations are used to develop a stiffness control scheme and task specific autonomous path planning for the purposes of singularity avoidance. The flexible body dynamics of the 3-3 and 6-6 SPM have been explored using finite element techniques [14], and an analytical vibration analysis of the 6-6 SPM has been conducted by considering the links as linear springs that only allow deformations in the axial directions [15]. Some preliminary experimental modal analysis of a 6-3 SPM has also been performed [16, 17]. In summary, a survey of the available literature on PKMs reveals a deficiency in the area of structural dynamics. The identification of structural stiffness, damping, resonant modes, and mode shapes is necessary to improve the design and control methodologies

for PKMs, and is especially relevant to machine tools based on parallel architectures.

In this paper a methodology for modeling the structural dynamics of parallel kinematic machines is presented. The purpose of the research is to develop a methodology for identifying the structural dynamic parameters of PKMs. The scope includes the derivation of an analytical model for simulating the vibration response and modal parameter configuration dependencies of a PKM. This model combines rigid-body and flexible-body dynamics using a component mode approach, and yields a set of linear ordinary differential equations (ODEs) that can be used to explore several of the issues associated with the structural dynamics of PKMs. The accuracy of these results is verified through experimental modal testing and analysis. The resulting model provides an effective means to evaluate machine performance, to guide the design process, and ultimately to improve control schemes.

THEORETICAL DEVELOPMENT

The PKM consists of a platform moved via a set of actuated kinematic chains connected between the platform and base. Figure 1 shows representative kinematic topologies of PKMs. The platform's rigid-body motion is achieved in one of three basic ways: (1) changing link lengths (extensible kinematic chain, Figure 1(b)), (2) changing the link orientation (Delta-like kinematic chain, Figure 1(c)), or changing the base joint locations (b_i) with fixed link lengths (Triaglide-like, Figure 1(d)). To encompass these three topologies in the structural dynamic model development, each kinematic chain (KC) is modeled using two distinct links, see Figure 2. Therefore, the intermediate joints in these kinematic chains can be either spherical, universal, revolute, prismatic or cylindrical joints. Then, for each pose of the platform, each i^{th} KC configuration can be defined in terms of the corresponding angle (α_i), platform joint location (p_i) and base location (b_i).

In this paper, the PKM's structural dynamics is formulated by examining the virtual displacements of the platform (position and orientation),

$$\underline{q} = (\delta x_c \quad \delta y_c \quad \delta z_c \quad \delta \phi \quad \delta \theta \quad \delta \psi)^T, \quad (1)$$

from a given pose. The platform is modeled as a rigid body and the links are modeled as flexible bodies. The individual links connecting the base to the platform are modeled as Euler-Bernoulli beams. Component mode synthesis techniques are used to relate the boundary conditions of the links to the motion of the platform.

Thus, assuming small deflections, the principle of superposition, sufficient friction in the joints yielding local boundary conditions to be those of a cantilever beams, the corresponding elastic axial and transverse deflections in the links are defined in $(\mathbf{u}_{2i}, \mathbf{v}_{2i}, \mathbf{w}_{2i})$ or in terms of corresponding displacements and rotations $\underline{\chi}_{Li}^* = [\mathbf{u}_i, \mathbf{v}_i, \mathbf{w}_i, \theta_{ui}, \theta_{vi}, \theta_{wi}]^T$ at point p_i . The total kinetic energy and potential energy (or

energy due to strain) is a sum of the individual link's energies and the platform energies. Introducing the constraints and eliminating unnecessary conditions, and using shape functions consisting of polynomial sums, the kinetic and potential energies for each i^{th} pair of links can be expressed, respectively, as

$$T_{Li} = \frac{1}{2} \underline{\dot{\chi}}_{Li}^{*T} M_{Li}^* \underline{\dot{\chi}}_{Li}^* \quad \text{and} \quad U_{Li} = \frac{1}{2} \underline{\chi}_{Li}^{*T} K_{Li}^* \underline{\chi}_{Li}^* \quad (2)$$

where

$$M_{Li}^* = \Gamma_{Li}^{*T} M_{Li} \Gamma_{Li}^* \quad \text{and} \quad K_{Li}^* = \Gamma_{Li}^{*T} K_{Li} \Gamma_{Li}^* \quad (3)$$

The Γ_{Li}^* is a constraint matrix which is a function of the boundary conditions and α_i . The M_{Li} and K_{Li} are the assembled mass and stiffness matrices for the link pairs prior to introducing the constraints.

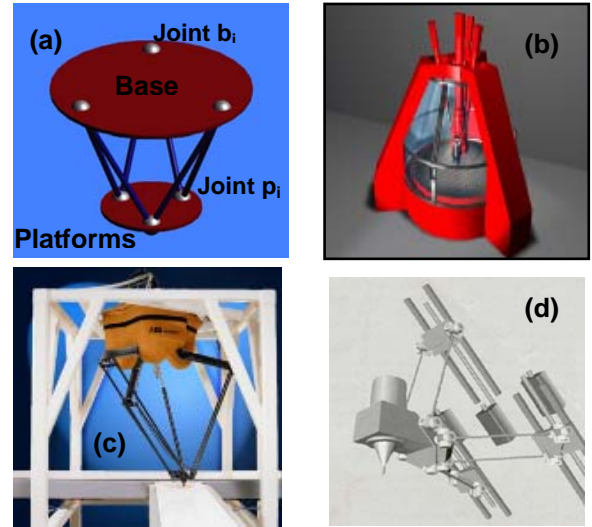


Figure 1: PKM Configurations:
[Top is base and bottom is platform.]

The Lagrangian approach is used to develop the equations of motion from expressions for the potential and kinetic energy of the system due to both the link pairs and the platform (K_p, M_p). Using \underline{q} as the generalized coordinates, the total kinetic energy (T) and potential energy (U) of the system can be expressed as follows, respectively.

$$T = \frac{1}{2} \underline{\dot{q}}^T M_p \underline{\dot{q}} + \sum_{i=1}^N \left(\frac{1}{2} \underline{\dot{q}}^T \Lambda_i^T M_{Li}^* \Lambda_i \underline{\dot{q}} \right) = \frac{1}{2} \underline{\dot{q}}^T M \underline{\dot{q}} \quad (4)$$

$$U = \frac{1}{2} \underline{q}^T K_p \underline{q} + \sum_{i=1}^N \left(\frac{1}{2} \underline{q}^T \Lambda_i^T K_{Li}^* \Lambda_i \underline{q} \right) = \frac{1}{2} \underline{q}^T K \underline{q} \quad (5)$$

The Λ_i is the constraint matrix mapping the coordinates from the local coordinates to set of generalized coordinates. I.e.,

$$\underline{\chi}_{Li}^* = \Lambda_i \underline{q}. \quad (6)$$

The result is a linear system of equations in six degrees of freedom. The below equation is the compact expression for the equations of motion.

$$\underline{M}\ddot{\underline{q}} + \underline{K}\underline{q} = \underline{Q} \quad (7)$$

The mass matrix (\underline{M}) and the stiffness matrix (\underline{K}) each include the both of the corresponding contributions due to the kinematic chains and the platform. The 6-vector of the generalized forces (\underline{Q}) includes the contributions due to both the applied loads on the platform and the actuator torques/forces in the kinematic chains. Note, due to page limitations, the detailed expansion of the above matrices and equations are too large to include in the paper. The reader is referred to reference [18] for greater detailed derivations.

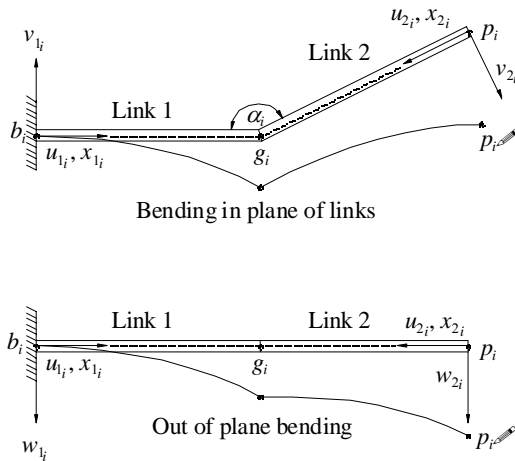


Figure 2: Deformation of a Kinematic Chain (b_i joint with base, p_i joint with platform, (u_i, v_i, w_i) local displacement coordinates).

EXPERIMENTAL VALIDATION

In this section, the theory is compared with the results of modal testing performed on the Hexel Tornado 2000 located at Sandia National Laboratories in Albuquerque, New Mexico.

Experimental Setup and Assumptions

Based on the architecture of the SPM, the Sandia Hexel Tornado 2000 (see Figure 3(a)) was designed for use as a milling machine. This particular PKM is a 6-3 mechanism, and possesses a platform that is maneuverable in 6 degrees of freedom (DOF). Each kinematic chain is connected to the base by a joint combination of universal and prismatic joints, and to the platform by a spherical joint (referred to as a bifurcated ball joint). According to the design of this machine, the platform joints are located at the vertices that define an equilateral triangle. The base joints form the vertices of a semi-regular hexagon as illustrated in Figure 3(b). Position and orientation

of the platform is accomplished through actuated extension of the kinematic chains (KC). To simplify the calculations associated with the mass moment of inertia terms, the mass distribution within the platform is assumed to be homogenous and is modeled as a solid circular cone.

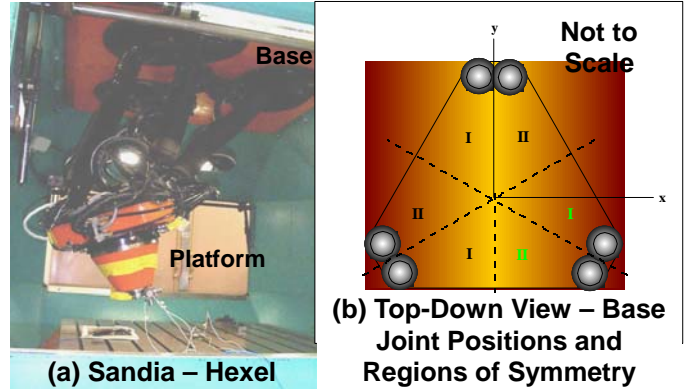


Figure 3: Hexel Tornado 2000.

Modal testing of the Sandia Hexel PKM was conducted using a specially-tuned modal impact hammer, six tri-axial accelerometers, and a data acquisition system with signal conditioning (including gain control and anti-aliasing) and an 8-channel capacity. The experimental setup is depicted in Figure 4. Once the machine was moved into a desired test configuration, the KC servos were locked and the accelerometers were placed in locations on either the KCs or tool-tip. Due to the limitations of the channel count, only two of the six tri-axial accelerometers could be connected at any given time. To avoid having to perform computationally intensive and often unreliable transformation operations on the acceleration data, the accelerometers were mounted to the structure with their axes either parallel or anti-parallel to the axes of the global machine controller coordinate system. Accelerometers were positioned along the KCs using spherical aluminum fixtures that were designed to clamp onto the KCs and provide a surface that would permit proper orientation; three locations were used per KC. Since it was discovered that the ceramic bearings in the spindle of this particular machine cannot sustain a static load, the tri-axial accelerometer mounted at the tool-tip was fastened to a threaded stud that was inserted into a custom fixture that could be attached to the spindle flange.

Data Collection

After the machine was moved into position and instrumented with accelerometers as described above, the structure was excited by striking the spindle shell (in the vicinity of the tool-tip) with the modal hammer. A separate set of data was collected for hammer hits directed along each of the machine controller coordinate system axes. In this case, the measurements were created using a single-input multiple-

output (SIMO) approach, and provided three reference frequency response functions. As a result of this testing, a total of 171 frequency response functions were generated per configuration. Five averages were used in the data acquisition process, and the criteria for rejection included observable multiple impacts, poor coherence (a statistical measure that can be used to identify regions of noisy and non-linear data), and either an underloaded or overloaded trigger.

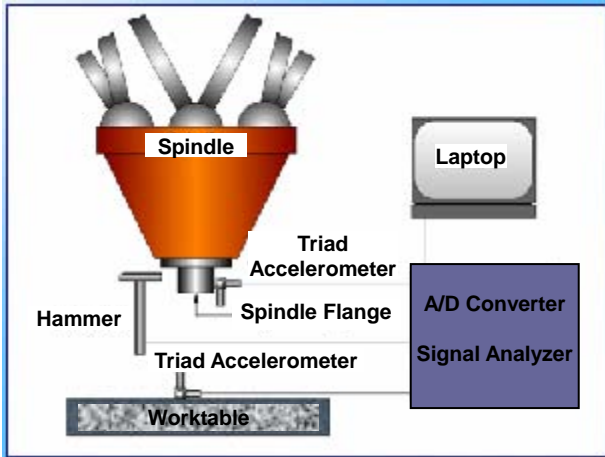


Figure 4: Illustration of Experimental Setup.

PKM Test Configurations

For the modal survey, it was assumed that the configuration dependency of the structural dynamic response for the machine could be fully mapped by examining only the regions indicated in the Figure 3(b)'s graph (regions I and II). That is, the geometry of the mechanism can be subdivided into six zones (designated by I and II) that are symmetric within the x and y planes. The regions selected for the modal survey have been highlighted in Figure 3(b), two lower right regions.

Test points were then defined at the vertices of a multi-tiered polar grid (in the xy plane). The modal survey consisted of a total of 27 different machine configurations. These test positions were selected on the basis of workspace boundaries and symmetry of the machine geometry with respect the global x and y planes. A graphical depiction of the location of the test points with respect to the mechanism workspace is given by Figure 5. To ensure acquisition of the acceleration data is conducted in global coordinates, the spindle was kept level for all test positions.

Modal Analysis

In the analysis of the experimental data, several modal parameter estimation techniques were used, with varying degrees of effectiveness. The estimation routines included the eigensystem realization algorithm (ERA), direct parameter estimation, and peak-picking. Although both the peak-picking procedure and the ERA performed reasonably well in terms of providing an accurate fit to the modal data, the first of these two algorithms was eventually selected over the second

because of its ability to produce a slightly more consistent set of results with respect to the selected frequency range.

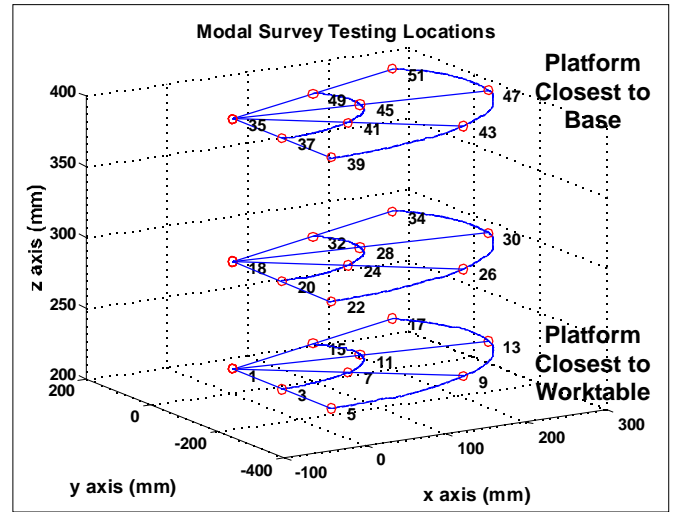


Figure 5: Modal Survey Test Positions.

MODAL ANALYSIS AND ESTIMATION RESULTS

To facilitate the estimation process and implementation of the theory, several computer programs were written in the MATLAB programming language. The first of these programs was an automated peak-picking algorithm that was designed to search the imaginary portion of a set of frequency response functions (FRFs) for possible resonant frequencies. In the process of determining of the number of potentially viable modes, only frequencies within the range of 0 - 500 Hz were considered and peaks measuring less than 10 percent of the maximum peak value were excluded. The parameters for modes within 5 Hz of one another were averaged. Damping ratios were obtained using an iterative curve-fitting technique, and directional stiffness associated with each mode and mode shape were found using a recursive routine that accounts for the effects of other modes. The modal stiffness terms were then calculated by finding the resultant displacement for each mode, and using the directional stiffness to calculate an equivalent stiffness. This effectively reduces to the formula for springs in series.

Figure 6 illustrates the effectiveness of the curve-fitting process for a well-defined set of peaks. The correlation coefficient for this particular set of curves is 0.92, which indicates that the estimation results are closely correlated with the actual experimental data. It should be noted that for this particular data set, the z direction (3rd column of plots) appears to possess the highest stiffness, and contributes little, if any, useful information to the estimation process. This is a trend which is relatively consistent for the configurations that were tested. It should also be noted, at this time, that FRFs which are excessively noisy or exhibit closely-spaced modes will detract

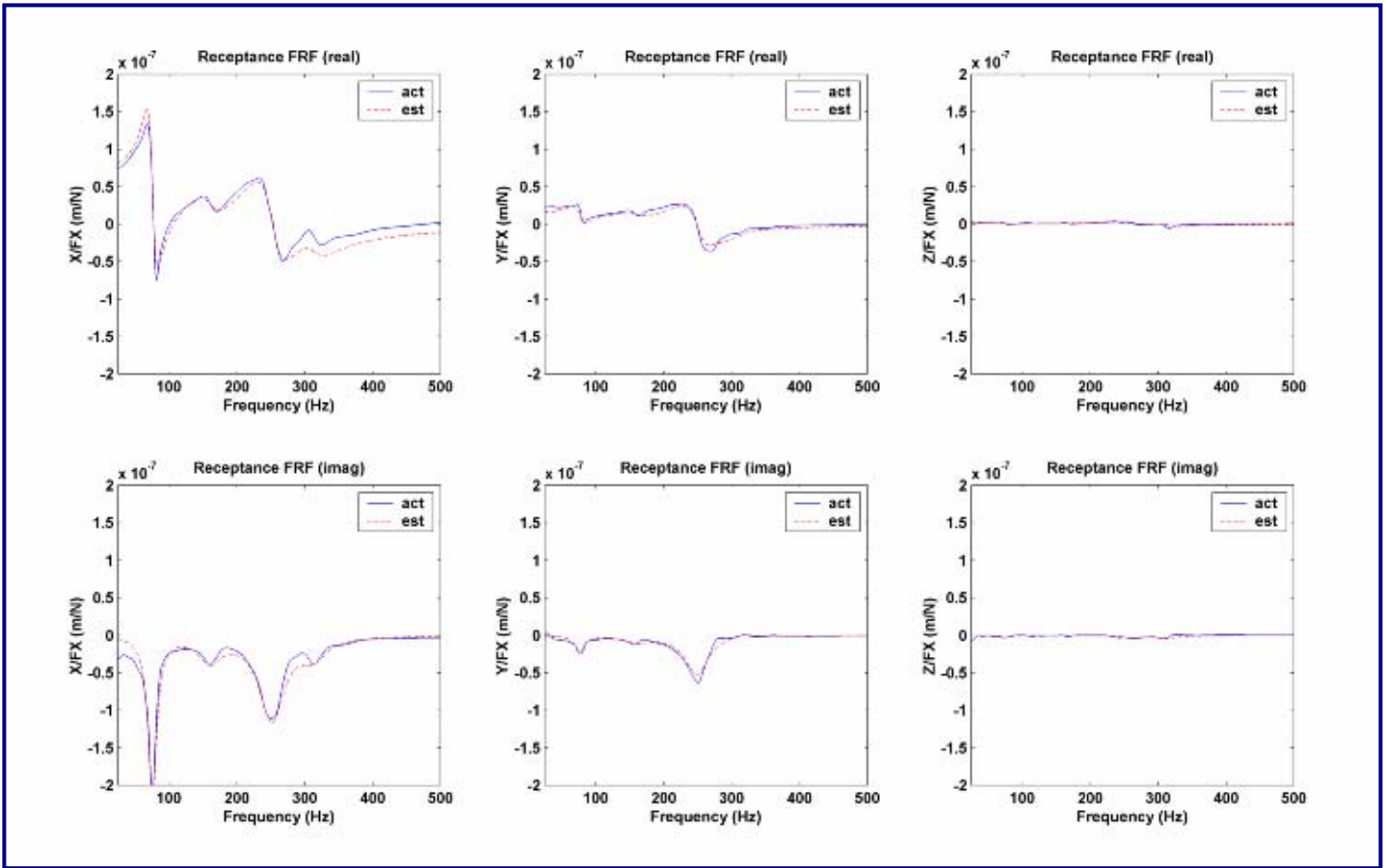


Figure 6: Modal Parameter Estimation Results for Test Configuration 1

from the accuracy of the estimation scheme, particularly in the ability to correctly identify modes and mode shapes

THEORETICAL VERSUS EXPERIMENTAL RESULTS

With the estimation complete, the analytical model was tuned to provide the closest match for the two lowest predicted modes. This was accomplished by changing the platform mass, rather than the material properties that are used to calculate the KC stiffness. There were several reasons for tuning the model in this manner, with the primary reasons being that it was only necessary to change one parameter, and that the platform mass was not known to any degree of accuracy to begin with (estimates have ranged from 100 lbs to 250 lbs).

To determine the effectiveness of the modeling approach, the modes generated by the theory are now compared to the modes estimated from the experimental data using several criteria. The modal assurance criterion (MAC) is essentially a dot product of the mode shape vectors that has been normalized to provide an answer between zero and one (with a value of one indicating a perfect match). The MAC was calculated

using the following equation, where Φ_{the} and Φ_{est} represent the theoretical and estimated mode shapes, respectively.

$$MAC = \frac{(\Phi_{the}^T \Phi_{est})^2}{(\Phi_{the}^T \Phi_{the})(\Phi_{est}^T \Phi_{est})} \quad (8)$$

Other criteria included proximity of the two frequencies and observability of the estimated mode.

Tables 1 – 2 compare the theoretical and experimental results for representative test configurations, where the percent difference was theoretical measured relative to the experimental. A shaded cell block indicates that the mode was estimated with low confidence, and is accompanied by a superscript character which provides the reason why. Superscript a indicates that either the magnitude of the peak of the imaginary portion of the FRF at the resonant frequency is less than $0.5e-7$ m/N, or the FRF was excessively noisy. Superscript b indicates that the difference in MAC values for other modes occurring within a range of 5 Hz differ by more than 0.5, or that the calculated MAC value was less than 0.5. Superscript c indicates that the estimated mode is one of two modes within 10 Hz of one another and occurring within the

same data set, and having the same phase (in this case, two separate modes that occur near the same frequency are indistinguishable when considering only one data set).

that there is a good correlation for the higher modes, the results obtained by the estimation process are often not convincing enough to conclude that a positive match has been made.

Table 1.
Resonant Frequencies - Position 1

Mode	f_n (Hz) Theoretical	f_n (Hz) Experimental	Percent Difference (%)	MAC
1	76	76	0.0	0.988
2	76	75	1.3	0.990
3	161	163 ^{ab}	-1.2	0.871
4	247	252 ^b	-1.2	0.751
5	268	250 ^{ab}	6.3	0.001
6	283	314 ^{ab}	-9.9	0.045

Table 2.
Resonant Frequencies - Position 9

Mode	f_n (Hz) Theoretical	f_n (Hz) Experimental	Percent Difference (%)	MAC
1	61	65	-6.2	1.000
2	72	73 ^b	-1.4	0.481
3	142	128 ^a	10.9	0.996
4	222	236	-5.9	0.640
5	256	–	–	--
6	295	–	–	--

These tables show that the theory was successful in predicting the two lowest modes, but was less effective in predicting the higher modes. Although it may appear at times

Because of this, the discussion that follows focuses mainly on the apparent trends and behavior of the two lowest modes.

Modal Analysis – Regional Trends

The average percent differences for modes 1 and 2 are 3.1% and 3.5%, respectively. The average MAC values for modes 1 and 2 are 0.974 and 0.744, respectively. This indicates a good correlation for these two modes, not only for frequency, but also for mode shape. Referring to Figure 5, examining separately the data for each of the xy planes at which measurements were taken reveals that the poorest correlation for the mode shapes (MAC values) occurs at test configurations 6, 15, and 25 for the first fundamental mode, and configurations 6, 15, and 24 for the second fundamental mode. With the exception of configuration 25, all of these configurations are located at the same x and y coordinates.

A further examination of the MAC values shows that the best correlation of theoretical and estimated mode shapes along a given direction occurs at the test configurations located along the y-axis of the machine, where the average MAC value for the first mode is 0.993 and the average MAC value for the second mode is 0.981. The worst correlation for MAC values (again considering the three xy planes of data separately) lies along the direction that includes test configurations 6, 7, 15, 16, 24, and 25. For the first mode, the average MAC value is 0.948; for the second mode, the average MAC value is 0.534.

In contrast with the MAC values, the frequency correlation for the first two modes does not indicate any particular region of the workspace for which there exists a discrepancy in the theory and the estimates. The poorest overall match occurs for

the data plane closest to the base, with an average percent difference of 5.0% for the two lowest modes. In comparison, the lowest and middle planes yield 3.0% and 1.8%, respectively. Examples of near perfect matching between the frequencies predicted by the theory and the frequencies determined from the experimental results include configurations 1, 13, 16, 25, and 27, where the percent differences for the first mode are less than 0.5% and the MAC values are greater than 0.90.

The theory indicates that there is little change in the frequency of the two lowest modes along lines of constant radius (with respect to the center of machine geometry). Also, as would be expected, frequency decreases with increasing radius and increases as the distance between the platform and the base decreases. These results are not surprising since the system stiffness is inversely proportional to the KC lengths. A more detailed look at these trends, as well as trends in stiffness is provided in later section.

Configuration Bias: Theory versus Experimental

Another observation that can be made while examining the data in the tables is that the frequencies predicted by the theory are consistently lower than those identified in the parameter estimation process for the measurements taken with the spindle situated 217 mm above the worktable. Conversely, the predicted frequencies are consistently higher than their experimental counterparts for measurements taken with the spindle 394 mm above the worktable. This suggests that the actual variation in stiffness for the machine is less than that of the model. Although it has not been attempted for this paper, it is possible that this behavior could be incorporated into the analytical model by reevaluating the boundary conditions used to develop the shape functions.

Mode Shapes

To conclude and to provide an example of the types of mode shapes predicted by the theory, a few representative mode shape plots are now given. Figure 7 depicts the mode shapes of mode 1 for test configuration 1. In this figure, the static configuration of the machine is depicted using solid lines, and the deflected position is depicted using dashed lines. It was found that the two lowest modes result in what appears to be a translation of the platform in either the x or y direction. Similarly, the fifth mode indicated a translation of the platform in the z direction. It seems reasonable that this mode is one of the highest modes since the z direction is one of the most stiff directions due to the physical arrangement of the PKM KCs. It should be noted that the manufacturers of PKMs for various applications have recently taken notice of the highly directional stiffness that tends to result from the existing PKM architectures, and have apparently begun investigating ways in which the joint configurations and types can be modified to provide a higher stiffness in the direction required by the specific task for which they are designed. This would also tend to suggest that a machine with a joint arrangement such as the

Sandia Hexel Tornado 2000 would be best suited to operations in which the cutting tool is moving in the z direction. Mode 3 appears to be a rotational mode in which the platform twists about the z axis. Modes 4 and 6 are combinations of rotation and translation, and occur in both the x and y directions.

TRENDS VERSUS PKM CONFIGURATIONS

The above results indicate that the resonant frequencies within the region of modal tests vary as a function of machine configuration. To understand how modal parameters can change with the platform position and orientation, the following is a summary of the investigation of a few issues concerning stiffness that have been raised by others in the machine tool community. All these results are purely theoretical and relate specifically to the geometry of the Hexel Tornado 2000.

Frequency Trends

First it was found that the resonant frequencies increase as the distance between the platform and the base decreases. This is a reasonably intuitive result that makes sense when one considers that the stiffness of the KC is proportional to the inverse of the KC length. The results also revealed a pronounced trilateral symmetry that appears to be closely related to the regions of machine symmetry that were discussed above. This effect is especially apparent for the higher modes, particular in the horizontal orientation of the platform. That is, the resonant frequency plotted as a function of spindle position displayed a high degree of symmetry in the radial direction of the workspace. The peak values for the first four modes tend to be located at or near the center of the workspace. In contrast, the peak values for the fifth and sixth modes tend to be found on the periphery of the workspace. A likely explanation for this behavior can be found in the stiffness matrices for the links. Comparatively, the bending and torsional stiffness are much lower than the axial stiffness. Physically, this suggests that the lower modes are probably due to a combination of rigid body motion of the platform and bending (or torsion) in the links. In the same sense, the higher modes are more likely attributable to the axial deflections occurring in the links.

In contrast, the following provides examples of how the resonant frequencies vary in cases where the platform has been rotated away from its original horizontal orientation. This illustrates the effect of changing one of the Euler angles has on resonant frequencies. Overall, there is slightly more variation in frequencies. Results show that the peak values for the lowest modes are no longer located in the center of the workspace. Instead, they have shifted and the direction of this shift is dependent on the direction in which the platform is rotated (think of how the KCs either extend or retract to produce the different platform orientations and also of their orientation with respect to the platform). With the exception of the higher modes, the peak values remain approximately the same. For the higher modes, the values are slightly higher,

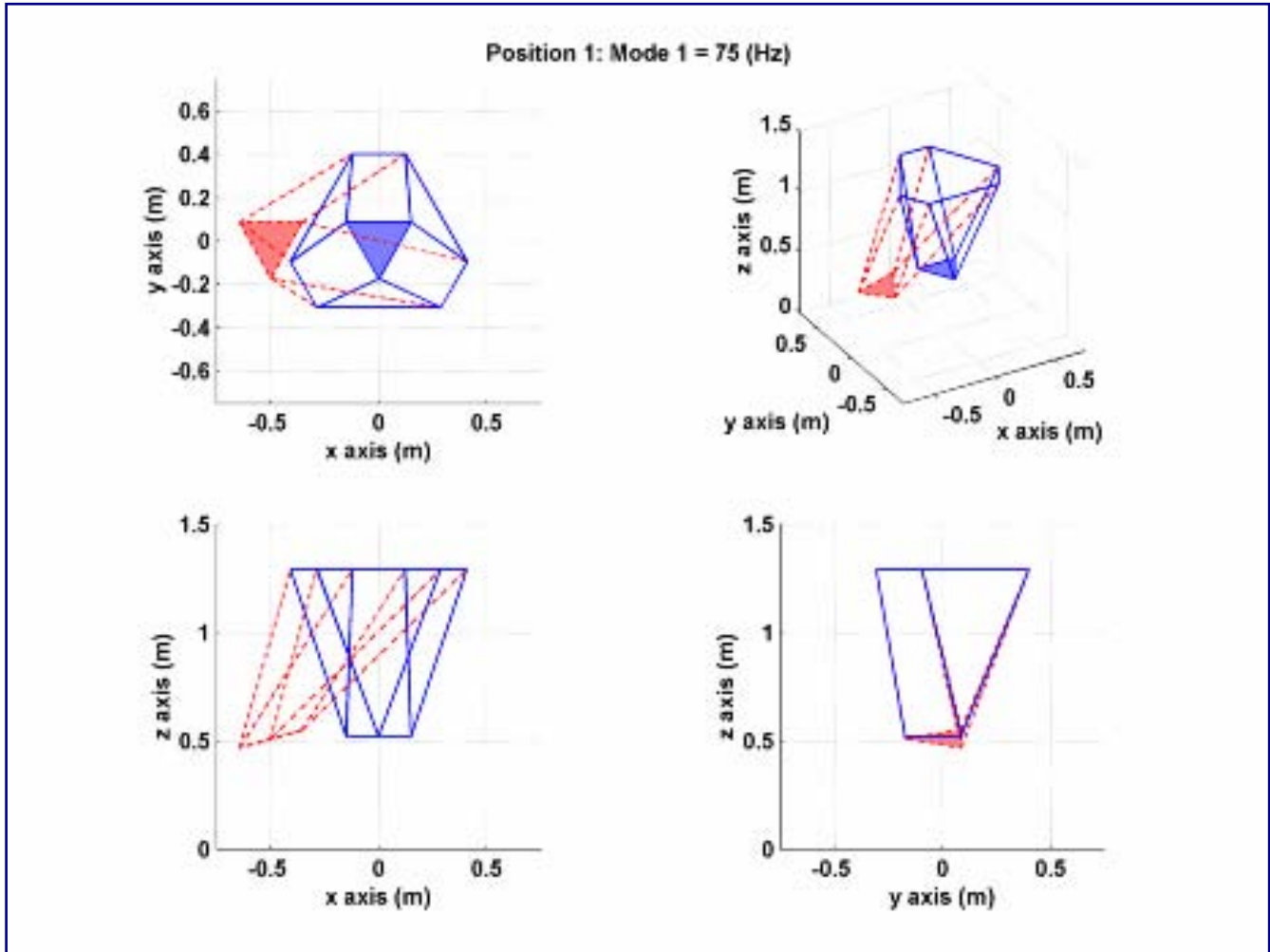


Figure 7: Mode Shape for Test Configuration 1 – Mode 1

indicating that these modes require more energy to excite them. It should also be noted that in comparing plots of the frequency variation for the two different values of the Euler angle α , that several of the modes appear to be mirror images of each other. Thus, the symmetry is bilateral and the frequencies tend to be lower than those produced for a level platform.

Stiffness Trends

Having examined the dependency of resonant frequency on machine configuration, the following are the findings of a study on the stiffness of the structure. This is approached in two ways: first, the stiffness of the overall structure is compared to the stiffness of the individual components; second, the theoretical modal stiffness is looked at in much the same way as were the resonant frequencies. In addressing the first of these items, it is assumed that an adequate representation of the strut stiffness is given by the axial stiffness. This assumption is made primarily to facilitate a comparison with the research of others, noting that previous studies on the stiffness of PKMs have been based on the notion that forces on the platform may

only be transmitted along the axes of the links. Comparing the axial stiffness of the six struts to the directional stiffness of the machine for several of the tested configurations, the results confirm the findings of others [2] by showing that the only direction in which the average stiffness of the KC is exceeded by the stiffness of the system is the z direction (the y direction for position 21 is the only exception).

For the lower modes, the stiffness is often highest in the center of the workspace. For these modes, the stiffness tends to decrease with increasing radius and increase with increasing z elevation. The fifth mode, which is associated with translation of the platform in the z (vertical) direction, shows a very sudden decrease in stiffness as the platform moves away from the center of the workspace. Overall, it can be seen that the modal stiffness can vary unpredictably and dramatically over the workspace. E.g., the stiffness of the first and second fundamental modes, which were found to be the most dominant in the experiments, can change substantially over small ranges of motion. Others (refer to previously cited reference) have noted how variations in stiffness throughout the workspace of

PKMs can lead to difficulties in controlling the mechanism in a way that will prevent undesirable results when performing machining operations. In considering this statement, it becomes clear that this variation of stiffness with machine configuration is an issue that needs to be addressed by the manufacturers and designers of PKMs if they are ever to establish the level of credibility in the marketplace that is necessary to successfully portray the PKM as a viable alternative to the conventional orthogonal machining center.

METHODOLOGY: MODELING AND IDENTIFICATION

Based on what has been presented, the overall methodology for modeling and identifying the structural dynamics of PKMs will now be described. The first step is to select the theoretical model that is most appropriate for the given PKM configuration type. To accommodate situations in which the friction in the joints is minimal, the boundary conditions used to establish the shape functions for the links can be changed. This will typically involve recalculating the generalized mass and stiffness terms, as well as formulating a new set of constraint equations. The second step is to acquire baseline tooltip modal data for use in reconciling the numerical values resulting from theory. Geometric symmetry of the mechanism can be used to minimize the set of data that is collected. The third step is to perform EMA on the modal test data and to compare the estimated parameters to those predicted by the theory. This can be accomplished by using a combination of MAC and frequency matching to verify which modes exhibit a high level of confidence in their correlation. Finally, the last step is to use the results to predict regions of good performance based on application needs.

DISCUSSION AND CONCLUSIONS

It has been shown that the theory is able to track the first two fundamental modes with reasonable accuracy. Finally, the dependency of resonant frequency and modal stiffness on machine configuration was investigated and followed by a discussion of a few of the issues that are related to these modal parameters. It has been shown that the variation of the frequency and stiffness parameters is dependent on machine configuration, and tends to reflect certain characteristics of the mechanism geometry, such as symmetry of the joint arrangements and symmetry due to platform orientations. In general, it was determined that stiffness and frequency increase as the distance between the platform and the base decreases, and decrease as the platform begins to approach the boundaries of the workspace. In confirming the research of others, it was shown that the theoretical stiffness of a single strut is often less than the theoretical stiffness of the machine in a given direction. It was also seen that bending of the links can play a significant role in the dynamics of PKMs.

ACKNOWLEDGMENTS

Funding provided by the National Science Foundation/Grant Opportunities for Academic Liaisons with Industry Program (NSF/GOALI) and matching funds from Sandia National Laboratories (SNL), Grant No. DMI-9800806. The authors extend their sincere appreciation for the technical support of Sandia colleagues, Donald Plymale, Lothar Bieg, Patrick Barney, and Bruce Swanson throughout this research.

REFERENCES

1. Fassi, I., and Wiens, G.J., 2000, "Multiaxis Machining: PKMs and Traditional Machining Centers," *Journal of Manufacturing Processes*, Vol. 1, No. 2, pp. 79-92.
2. Tlusty, J., Ziegert, J.C., and Ridgeway, S., 2000, "A Comparison of Stiffness Characteristics of Serial and Parallel Machine Tools," *Journal of Manufacturing Processes*, Vol. 2, No.1, pp. 67-76.
3. Do, W.Q.D., and Yang, D.C.H., 1988, "Inverse Dynamic Analysis and Simulation of a Platform Type of Robot," *Journal of Robotic Systems*, Vol. 5, No. 3, pp. 207-227.
4. Zhiming, J., 1993, "Study of the Effect of Leg Inertia in Stewart Platforms," *Proceedings of the IEEE Conference on Robotics and Automation*, Vol. 1, pp. 121-126.
5. Wiens, G.J., Shamblin, S.A., and Oh, Y.-H., 2002, "Characterization of PKM Dynamics in Terms of System Identification," *Journal of Multi-body Dynamics, Special Issue on Parallel Kinematic Machines*, Vol. 216, Part K, pp. 59-72.
6. Dasgupta, B., and Mruthyunjaya, T.S., 1998, "A Newton-Euler Formulation for the Inverse Dynamics of the Stewart Platform Manipulator," *Mechanism and Machine Theory*, Vol. 33, No. 8, pp. 1135-1152.
7. Geng, Z., Haynes, L.S., Lee, J.D., and Carroll, R.L., 1992, "On the Dynamic Model and Kinematic Analysis of a Class of Stewart Platforms," *Robotics and Autonomous Systems*, Vol. 9, No. 4, pp. 237-254.
8. Pang, H., and Shahinpoor, M., 1994, "Inverse Dynamics of a Parallel Manipulator," *Journal of Robotic Systems*, Vol. 11, No. 8, pp. 693-702.
9. Baiges-Valentin, I.J., 1996, "Dynamic Modeling of Parallel Manipulators," PhD. dissertation, University of Florida, Gainesville, FL, 226 pp.
10. Wiens, G.J., and Johnston, P.R., 1999, "Dynamic Performance of Parallel Kinematic Machines," *Transactions of the North American Manufacturing Research Institution of SME*, Vol. XXVII, pp. 311-316.
11. Liu, M., 1999, "Dynamics Analysis of the Stewart Platform Manipulator," *Proceedings of the International Symposium on Test and Measurement*, Int. Acad Publ., Beijing, China, pp. 920-923.
12. Lee, J. D., and Geng, Z., 1993, "A Dynamic Model of a Flexible Stewart Platform," *Computers and Structures*, Vol. 48, No. 3, pp.367-374.

13. Lebret, G., Liu, K., and Lewis, F.L., 1993, "Dynamic Analysis and Control of a Stewart Platform Manipulator," *Journal of Robotic Systems*, Vol. 10, No. 5, pp. 629-655.
14. Ramachandran, S., Nagarajan, T., and Prasad, N.S., 1992, "A Finite Element Approach to the Design and Dynamic Analysis of Platform Type Robot Manipulators," *Finite Elements in Analysis and Design*, Vol. 10, No. 4, pp. 335-350.
15. Yang, H., and Masory, O., "Vibration Analysis of Stewart Platform," Florida Atlantic University, Boca Raton, FL.
16. Hardage, D.S., and Wiens, G.J., 1999, "Modal Analysis and Modeling of a Parallel Kinematic Machine," *Symposium on Recent Advances in Machine Tools: Metrology and Modeling*, IMECE Proceedings of ASME: Manufacturing Science and Engineering, MED Vol. 8, Nashville, TN, November 14-19, 6 pgs.
17. Wiens, G., and Hardage, D., 1999, "Dynamics and Controls of Hexapod Machine Tools," *Parallel Kinematic Machines: Theoretical Aspects and Industrial Requirements*, edited by C. R. Boer, L. Molinari-Tossatti, and K. S. Smith, Springer-Verlag, London, pp. 217-225.
18. Hardage, D.S., 2000, "Structural Dynamics of Parallel Kinematic Machines," Ph.D. Dissertation, University of Florida, Gainesville, Florida.